PROPERTIES OF THE ψ RESONANCES*

M. Breidenbach

Stanford Linear Accelerator Center
Stanford University, Stanford, California, USA

ABSTRACT

Sharp peaks are seen in the electron-positron annihilation cross section corresponding to the ψ at 3.095 GeV and the ψ' at 3.684 GeV. Cross sections for the ψ and ψ' decay into hadrons, e^+e^- pairs, and $\mu^+\mu^-$ pairs are used to deduce the widths and quantum numbers of the ψ and ψ'. Studies of the decay modes are used to determine the G-parity of the ψ and the existence of a two-pion cascade decay from the ψ' to the ψ. No other narrow resonances have been found with masses between 3.2 and 7.6 GeV.

In early November of 1974 the total annihilation cross section for electrons and positrons into hadrons at high energy seemed essentially featureless. After the structure of the vector mesons the cross section decreased slowly with increasing energy. Within a month, this relatively simple picture had become somewhat chaotic due to the discovery of two very narrow resonances, the ψ at a mass of 3.1 GeV[1)] and the ψ' at a mass of 3.7 GeV.[2)] The most surprising features of these particles are their extremely narrow widths (or long lifetimes) for so massive states and the magnitudes of the peak cross sections. At the ψ, the experimentally observed cross section increases by a factor of more than 100 from that observed at a beam energy only 2.5 MeV lower. It seems that some basically new physics is manifesting itself, such as a new quantum number or selection rule. We will describe some of the properties of the ψ's as determined at SPEAR[3)] by the SLAC-LBL collaboration.[4)]

The data to be described were acquired with the SLAC-LBL magnetic detector, which is shown in Fig. 1 and described in more detail in Appendix I. Basically, it is a cylindrical detector 3 meters in diameter and 3 meters long, and has a uniform axial magnetic field of 4 kilogauss. The detector encompasses the full azimuthal coordinate and includes a solid angle of $0.65 \times 4\pi$.

* Work supported by the U.S. Energy Research and Development Administration.

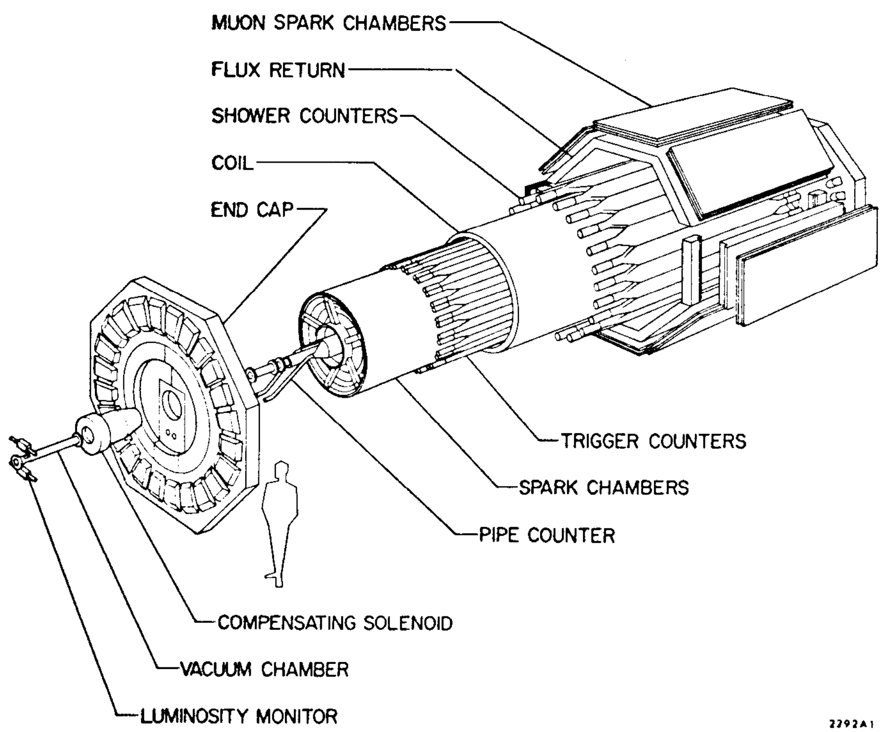

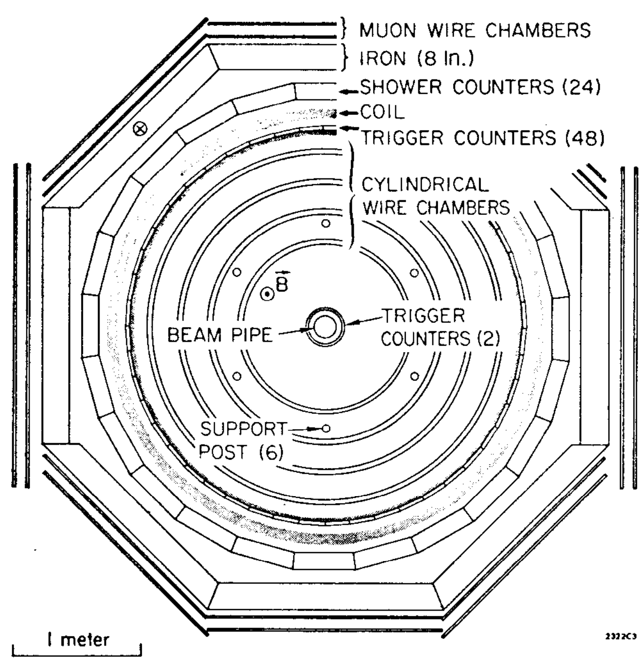

Fig. 1 The SLAC-LBL Magnetic Detector.
a) Telescoped view.
b) End view.

Charged particles with momenta greater than 100 MeV/c are detected, and two particles with transverse momenta greater than about 200 MeV/c are required for a trigger. Yields are normalized by measurements of Bhabha scattering at small angles (25 mrad). Backgrounds at the resonances are negligible (< 0.1%).

MEASURED CROSS SECTIONS AND DECAY WIDTHS

Measurements of the cross sections for the resonant decays into hadrons, e pairs, and μ pairs allow, with assumptions about the shape and quantum numbers of the resonant state, the calculation of the true resonant width and the partial widths for e pairs and μ pairs. The assignments of the quantum numbers will be deduced from interference effects between the resonant amplitude and the direct QED amplitude in the μ-pair channel.

Figure 2a shows the total cross section for hadron production σ_T versus center-of-mass energy $E_{c.m.} = 2 E_{beam}$ for the ψ.[5] The observed full width at half maximum (FWHM) is 2.6 MeV, which is the width expected from the convolution of a much narrower resonance shape, the inherent spectral resolution of the storage ring, and radiative corrections in the production of a virtual photon. Figures 2b and 2c show the cross sections for the final states $\mu^+\mu^-$ and e^+e^-,

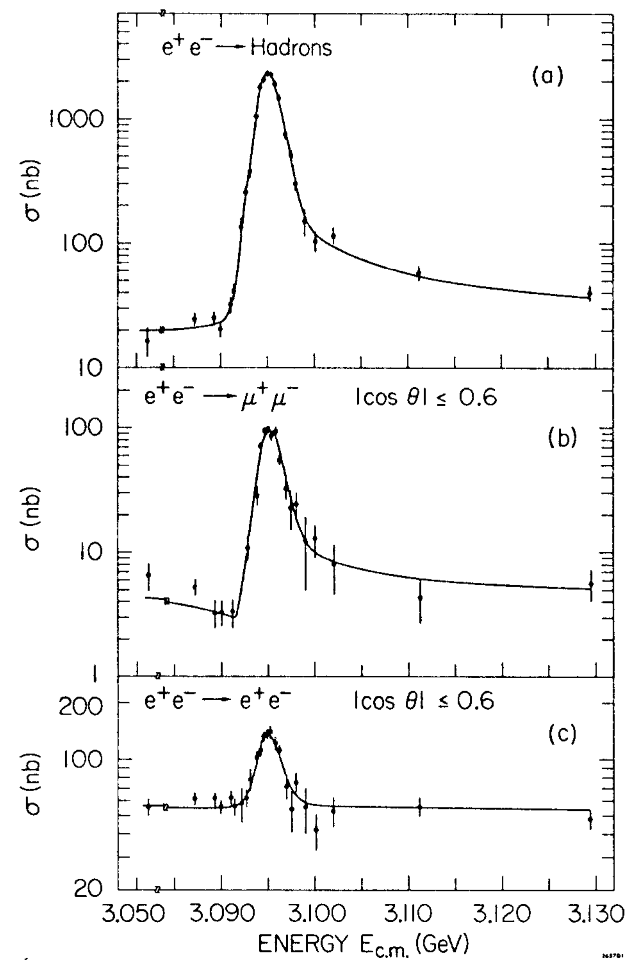

Fig. 2 Cross sections for the indicated modes in the vicinity of the ψ. Only the hadronic cross sections are corrected for detector acceptance. The curves show the fitted cross sections.

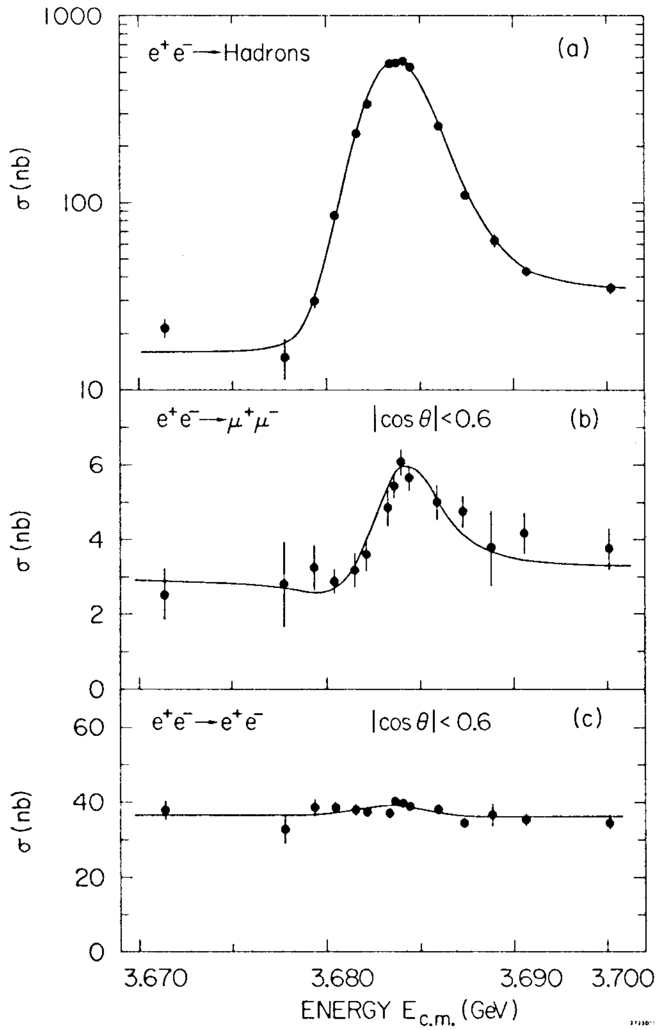

Fig. 3 Cross sections for the indicated modes in the vicinity of the ψ'. Only the hadronic cross sections are corrected for detector acceptance. The curves show the fitted cross sections.

respectively.[6] The cross sections are integrated over the angular region $|\cos\theta| < 0.6$, where θ is the angle between the outgoing positive lepton and the positron beam. The corresponding cross sections for the ψ'[7] are shown in Figure 3. The observed FWHM is about 4.6 MeV, which is also compatible with a much smaller true width. The peak cross section is about 550 nb, approximately one-quarter that of the ψ. The integrated resonance strengths, with radiative corrections, are:

$$\psi: \quad \Sigma_h = \int \sigma_h^{\psi}(E_{c.m.})\, dE_{c.m.} = 10{,}400 \pm 1500 \text{ nb-MeV}$$

$$\psi': \quad \Sigma_h = \int \sigma_h^{\psi'}(E_{c.m.})\, dE_{c.m.} = 3700 \pm 600 \text{ nb-MeV}.$$

The extraction of the leptonic cross sections for the ψ' is complicated by the large branching ratio for ψ' to ψ decay, followed by the subsequent leptonic decay of the ψ. The decay of the ψ' into leptons may be separated from the cascade decay by reconstructing the invariant mass of the lepton pair. This can be done if the detector has sufficient momentum resolution. Such a separation is shown in Figure 4. The e^+e^- pairs from the ψ may be seen above the radiative tail of the ψ' in Fig. 4a. The $\mu^+\mu^-$ pair separation is shown in Fig. 4b, and is very clean. The difference between the electron pairs and the muon pairs is that the resonant electron cross section sits on a QED background of about 37 nb[8] (electron pairs are produced from spacelike scattering processes as well as the annihilation of the e^+ and e^-), but the $\mu^+\mu^-$ pair cross section is on a background of only 3 nb. (The $\mu^+\mu^-$ pairs come only from annihilation.) Assuming μ-e universality, the resonant μ pair and e pair cross sections are equal.

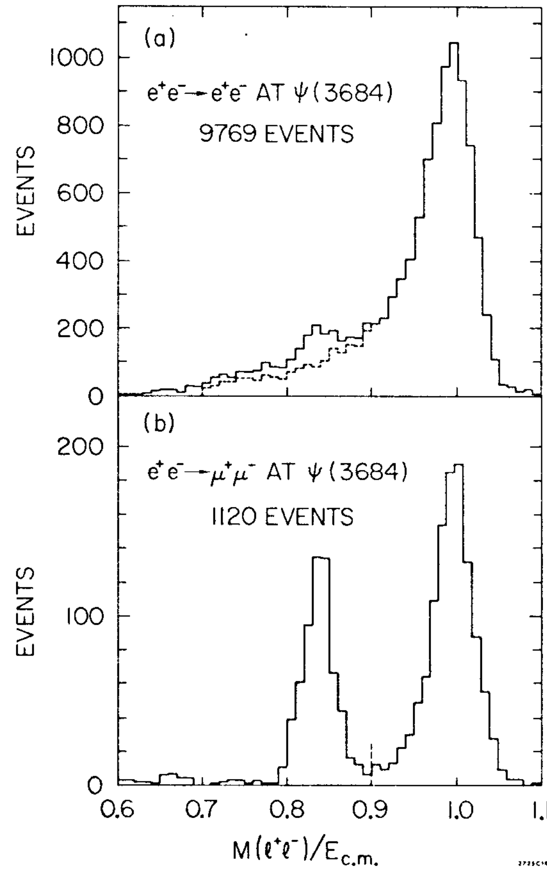

Fig. 4 Invariant mass of lepton pairs from the ψ'. The dotted lines indicate the cuts that were made.
a) $e^+e^- \to e^+e^-$.
b) $e^+e^- \to \mu^+\mu^-$.

These data may be used to calculate the true width Γ, as well as the partial widths for decays into hadrons, Γ_h; e^+e^- pairs, Γ_e; and $\mu^+\mu^-$ pairs, Γ_u for each of the resonances. If we assume that the resonance has a Breit-Wigner shape, then the resonant cross section σ_f for the decay to any set of final states f is

$$\sigma_f = \frac{(2J+1)\pi}{m^2} \frac{\Gamma_e \Gamma_f}{(E_{c.m.}-m)^2 + \Gamma^2/4} ,$$

where J is the spin of the resonance, m is the resonance mass, and Γ_f is the width to the set of final states. Γ is the total width for the decay to all final states. If this expression is integrated over the center-of-mass energy, it may be compared to the integrated experimental cross sections (after appropriate radiative corrections)[9] without explicit dependence on the storage ring energy resolution. Thus:

$$\Sigma_f = \int \sigma_f \, dE_{c.m.} = \frac{(2J+1)\,2\pi^2}{m^2} \frac{\Gamma_e \Gamma_f}{\Gamma} .$$

Then, assuming J = 1 (which will be justified shortly) and that $\Gamma = \Gamma_h + \Gamma_e + \Gamma_\mu$, i.e., there are no neutral modes, $\Gamma_e = \frac{m^2}{6\pi^2} \Sigma_{all}$, and $\Gamma = \Gamma_e \frac{\Sigma_{all}}{\Sigma_{ee}}$.

Since Σ_{ee} is small and sitting on a (relatively) large background, it is advantageous to assume μ-e universality and substitute $\Sigma_{\mu\mu}$ for Σ_{ee} in the expression for Γ, particularly at the ψ'. Alternatively, one may simultaneously fit the three cross sections to determine the mass and the widths. (Each resonance is done separately.) The fit folds the Gaussian energy resolution of the ring with radiative effects and a Breit-Wigner cross section. Also included are the effects of interference between the resonant channel $e^+e^- \rightarrow \psi \rightarrow f$ and the direct process $e^+e^- \rightarrow f$. The results of the two techniques agree, and the results are shown in Table I. The errors are mainly due to systematic uncertainties, such as uncertainty in the hadron detection efficiency, and are listed in the tables.

TABLE I

Properties of the ψ-particles as obtained from fit to cross sections σ_{HAD}, $\sigma_{\mu\mu}$, and σ_{ee}

	$\psi(3095)$	$\psi(3684)$
Mass	3.095 ± 0.004 GeV	3.684 ± 0.005 GeV
J^{PC}	1^{--}	1^{--}
$\Gamma_e = \Gamma_\mu$	4.8 ± 0.6 keV	2.2 ± 0.3 keV
Γ_H	59 ± 14 keV	220 ± 56 keV
Γ	69 ± 15 keV	225 ± 56 keV
Γ_e/Γ	0.069 ± 0.009	0.0097 ± 0.0016
Γ_H/Γ	0.86 ± 0.02	0.981 ± 0.003
Γ_μ/Γ_e	1.00 ± 0.05	0.89 ± 0.16

Errors accounted for: (a) statistical, (b) 15% uncertainty on hadron efficiency, (c) 100 keV setting error in $E_{c.m.}$, (d) 2% point-to-point errors, uncorrelated, (e) 3% luminosity normalization.

The full width of the ψ is about 70 keV, and that of the ψ' is about 225 keV. All of the widths in the table except the last row were calculated assuming $\Gamma_e = \Gamma_\mu$. This hypothesis of μ-e universality is tested in the last row, and good agreement with universality is found.

SPIN AND PARITY

If the resonances are eigenstates of P and C, there should be no asymmetry in the angular distribution of the leptonic decays. The front-back asymmetry for μ pairs as a function of energy is shown for the ψ and ψ' in Fig. 5. The

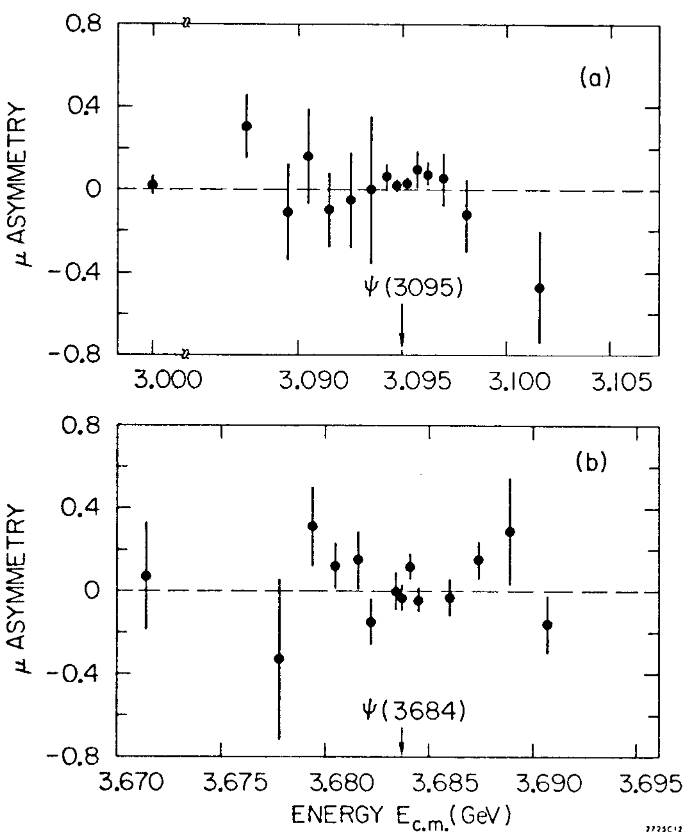

Fig. 5 The front-back asymmetry for $\mu^+\mu^-$ pairs
a) near the ψ
b) near the ψ'.

asymmetries are consistent with zero, indicating no significant violation of parity or charge conjugation, and that the resonances are not mixtures of states of opposite parity.

Since the ψ's are copiously produced in e^+e^- annihilation, one might expect them to couple directly to the annihilation photon and have the same quantum numbers, $J^{PC} = 1^{--}$. This assignment of J^{PC} would not be necessary if a ψ were produced by a direct interaction of the electron and positron.

If the ψ's couple directly to the photon, one would expect interference between the muonic decays of the ψ's,

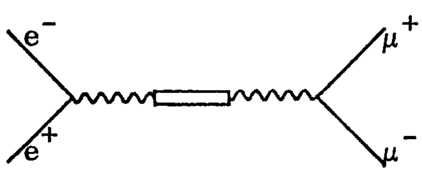

$$A = \left(\frac{(2J+1)\pi}{E_{c.m.}^2}\right)^{\frac{1}{2}} \frac{\Gamma_e}{m-E_{c.m.}-i\Gamma/2}$$

and the direct QED production of muon pairs

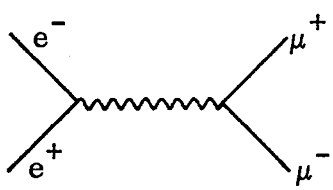

$$A = \left(\frac{3\pi}{E_{c.m.}^2}\right)^{\frac{1}{2}} \left(\frac{-2\alpha}{3}\right) .$$

These two amplitudes would interfere, yielding a cross section proportional to

$$\left| \frac{-2\alpha}{3} + \frac{\Gamma_e}{m - E_{c.m.} - i\Gamma/2} \right|^2 .$$

The addition is shown graphically in Figure 6, and it can be seen that there will be destructive interference at energies slightly below the peak.

In practice, the ratio of the μ-pair to e-pair cross sections is compared with predictions in order to eliminate systematic normalization errors. Such comparisons are shown in Fig. 7. The data are fully compatible with the hypothesis of interference, and disagree with the hypothesis of no interference (e.g., J = 0) by 2.7 standard deviations for the ψ and 4.9 standard deviation deviations for the ψ'. Because the detector does not cover the full solid angle, the observation of interference does not necessarily mean J = 1. (But because the detector is symmetric in space, and with respect to charge, and sums over spins, the observation of interference does imply P = C = -1.)

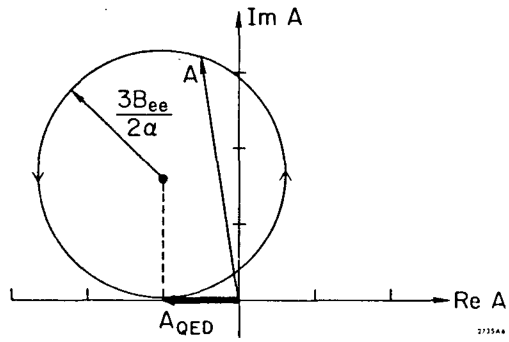

Fig. 6 Addition of interfering resonant and direct QED amplitudes.

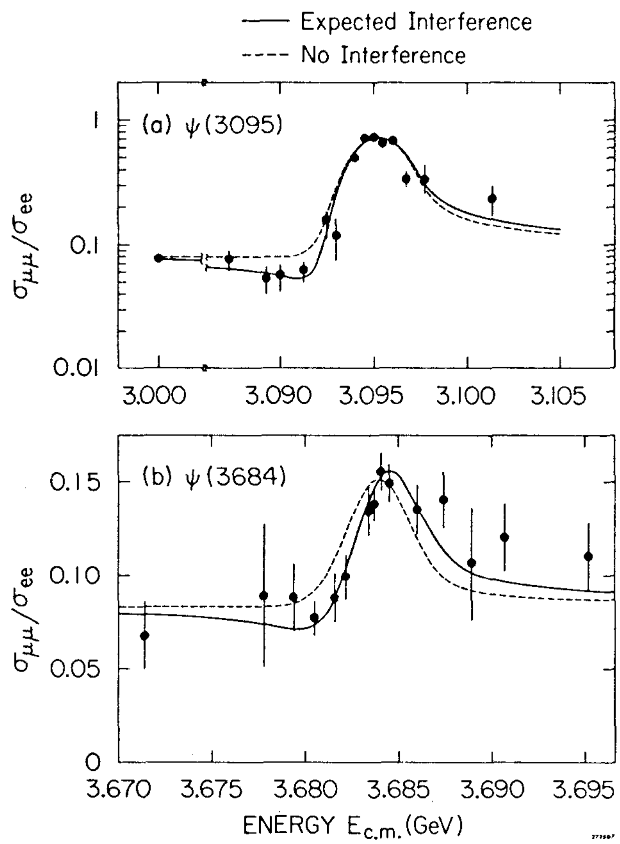

Fig. 7 The ratio of μ pair to e pair cross sections
a) near the ψ
b) near the ψ'.

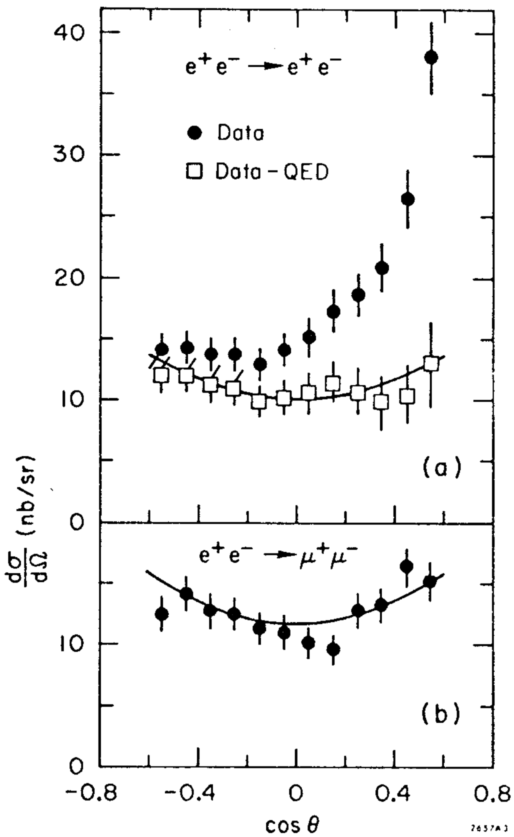

Fig. 8 a) The angular distribution of electron pairs at the ψ, $3.0944 < E_{c.m.} < 3.0956$.
b) The angular distribution of muon pairs in the same energy range.

However, spins 2 and 3 cause constructive interference (for the detector geometry) and generate predictions even further from the data than the J = 0 assumption.

Figure 8 shows the angular distribution for the leptonic decays of the ψ. For the e^+e^- pairs, the open boxes show the data with the QED contribution removed. The curves represent $1 + \cos^2\theta$. Figure 9 shows the angular distributions for the ψ'. The dashed curve is the cross section expected from QED, while the solid curves include the resonant contribution calculated from the widths discussed earlier. The angular distribution for both particles confirms the J = 1 assignment from the interference results.

ψ DECAYS

The hadronic decays of the ψ may be either direct decays

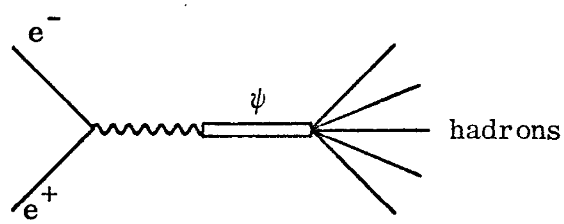

or "2nd order electromagnetic" decays

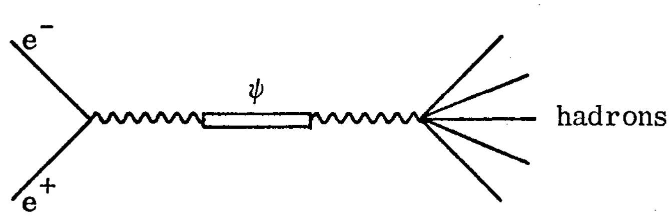

The G-parity of the ψ may be obtained by observing whether the direct decay of the ψ is into states containing even or odd numbers of pions. The photon in the "2nd order electromagnetic" decay does not have definite isospin and can decay into either even or odd numbers of pions.

The resonant muon pairs presumably come from a 2nd order decay

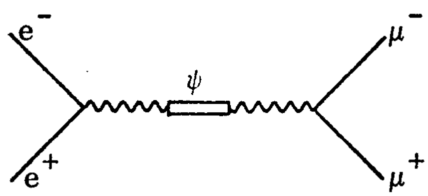

Away from the resonance, let us define $R_{off} = \frac{\sigma_h^{off}}{\sigma_\mu^{off}}$, where σ_h is the cross section for a particular hadronic channel and σ_μ is the $\mu^+\mu^-$ cross section. Similarly, define R_{on} as the corresponding ratio on the resonance. If all of the hadronic decays were 2nd order electromagnetic, then $R_{on} = R_{off}$. If there is a direct decay, $R_{on} > R_{off}$. In order to cancel most of the systematic errors, we will examine the ratio $\alpha = R_{on}/R_{off}$, so that $\alpha = 1$ for the second order process and $\alpha > 1$ for direct decays.

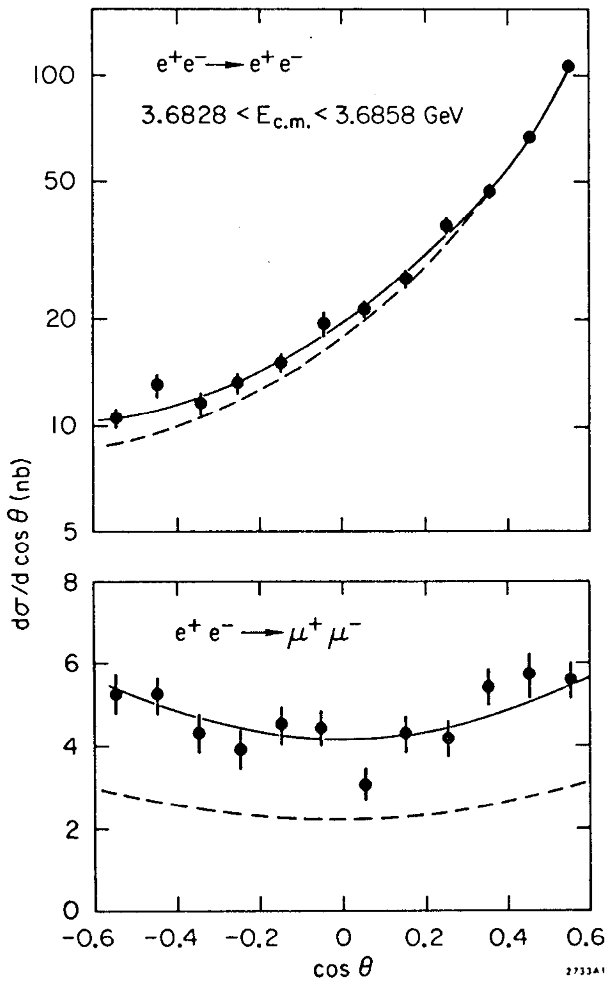

Fig. 9 a) The angular distribution of electron pairs at the ψ'.
b) The angular distribution of muon pairs at the ψ'.

The first step is to isolate the different multipion final states. Since the time-of-flight particle identification system does not isolate pions with momenta greater than about 650 MeV/c, the identification of exclusive states depends on energy and momentum balance for states with all particles observed, and on the existence of a missing mass peak for events with one missing neutral. Figure 10 shows the missing mass recoiling against four charged pions. At the resonance, a large peak is seen,[10] corresponding to $\psi \to \pi^+\pi^-\pi^+\pi^-\pi^0$. Off the resonance at $E_{c.m.}$ = 3.0 GeV, no peak is discernable and only an upper limit on the five-pion yield may be determined. Figure 11 shows the total energy in four-prong events at the ψ, assuming that each of the prongs is a π. The peak at 3.1 GeV is due to $\psi \to \pi^+\pi^-\pi^+\pi^-$, and the peak at 2.8 GeV is due to $\psi \to \pi^+\pi^-K^+K^-$. The 4π cross section at $E_{c.m.}$ = 3.0 GeV

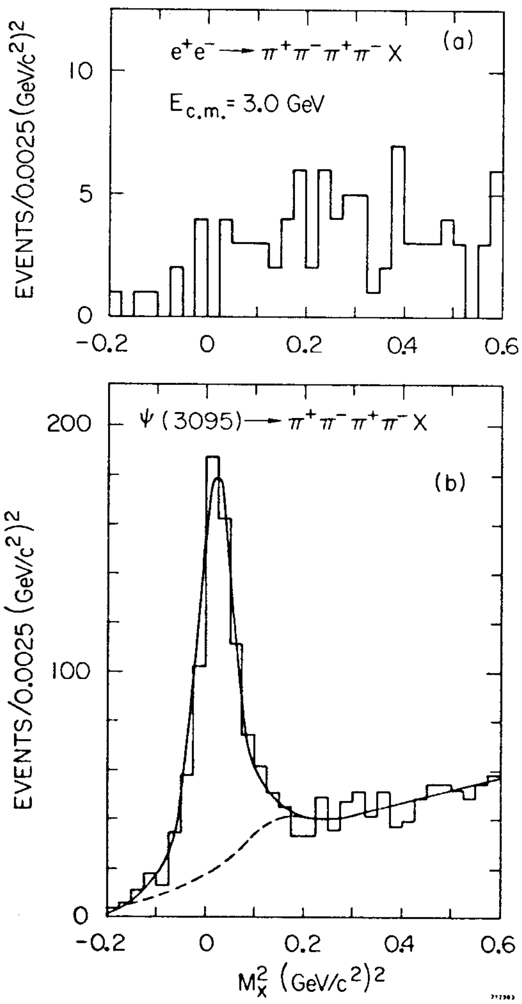

Fig. 10 The missing mass squared recoiling against four charged pions
a) at $E_{c.m.}$ = 3.0 GeV
b) at the ψ.

can be isolated in a similar manner.

In Figure 12, α is shown for final states containing from 3 to 7 pions. The states containing 4 and 6 pions have α = 1, the value expected from the "2nd order electromagnetic" decays, while

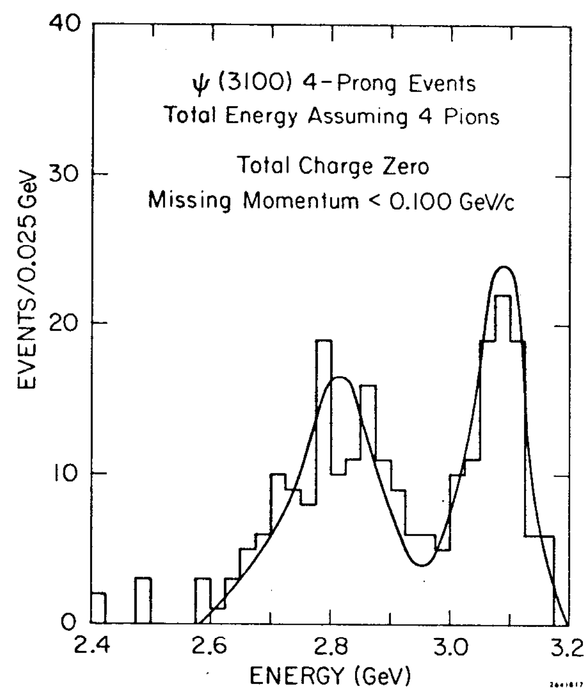

Fig. 11 Total observed energy in four-prong events at the ψ. The curve is a Monte Carlo fit to the data.

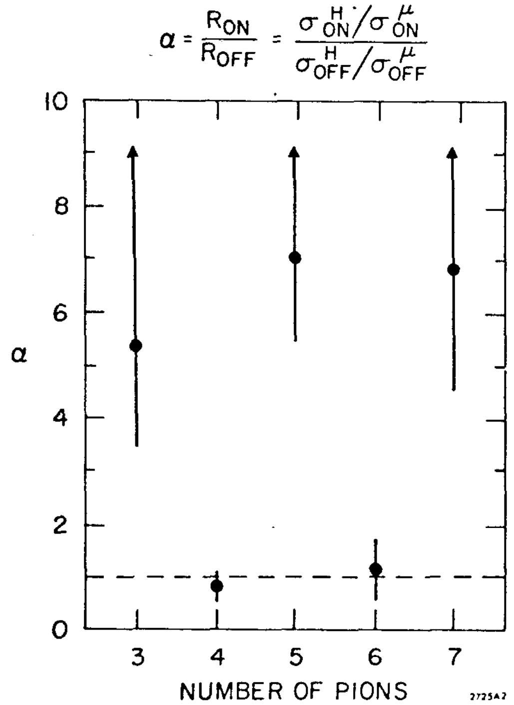

Fig. 12 Comparison of α for different multipion final states at the ψ (ON) and at 3.0 GeV (OFF).

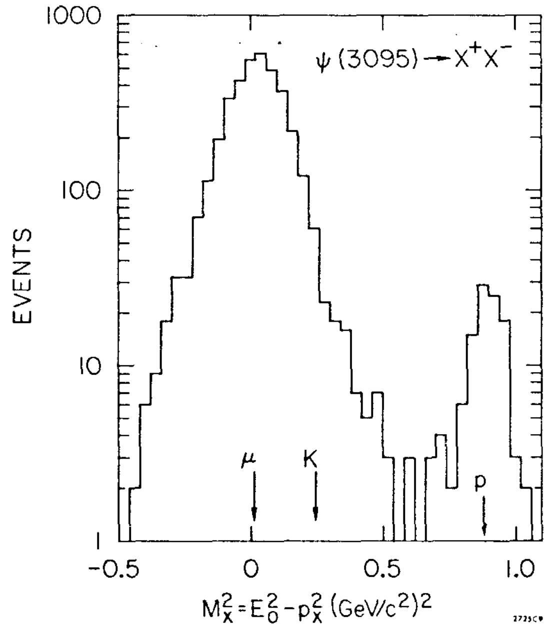

Fig. 13 Mass squared for collinear 2-prong events from the ψ. e^+e^- pairs have been removed by shower-counter pulse-height cuts.

the states containing odd numbers of pions have α greater than one. We conclude that the direct decay of the ψ is to states of odd numbers of pions and thus the G-parity of the ψ is odd. For final states having only pions, $G = C(-1)^I$, so the isospin of the ψ must be even. Also, the value of $\alpha = 1$ for the even number of pion states indicates that the ψ does not have direct leptonic decays.

Figure 13 shows the invariant mass distribution for the ψ decaying into a pair of charged particles. A peak corresponding to the $\bar{p}p$ decay is clearly visible. The absence of an observable peak off the resonance indicates that the $\bar{p}p$ mode is a direct decay of the ψ. Since the isospin of a $\bar{p}p$ state can be only 0 or 1, and since 1 is excluded by the odd G-parity, the isospin of the ψ must be 0.

Another technique to determine the isospin of the ψ is through the decay $\psi \to \pi^+\pi^-\pi^0$. Figure 14 shows the Dalitz plot for this decay, indicating that the dominant mode is $\rho\pi$. The horizontal, vertical, and diagonal bands correspond to the $\rho^-\pi^+$, $\rho^+\pi^-$, and $\rho^0\pi^0$ modes, respectively. Since these three modes occur with equal frequency, the I = 0 assignment is selected over I = 2, which

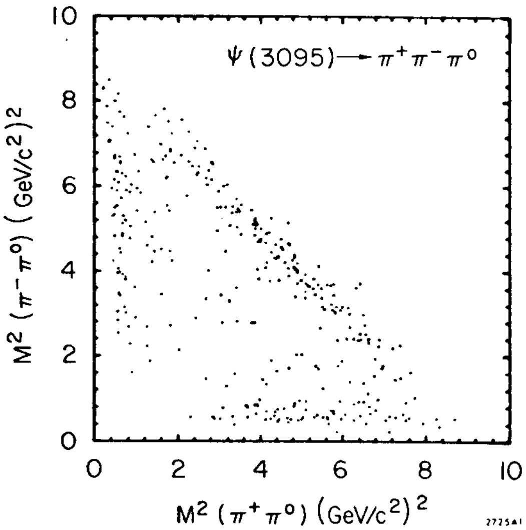

Fig. 14 Dalitz plot for the $\psi \to \pi^+\pi^-\pi^0$ decay.

would require $\rho^0\pi^0$, $\rho^+\pi^-$, and $\rho^-\pi^+$ to be in the ratio 4:1:1.

The study of the ψ decay modes is still incomplete. A "progress report" is shown in Table II. These decay modes offer a clue to the SU_3 nature of the ψ,[11] i.e., whether the ψ is an SU_3 singlet, the eighth component of an octet, or a mixture of the two, such as the ω or ϕ. For an SU_3 singlet, all decays into pairs of pseudo-scalar mesons are forbidden, e.g., $\psi \to \pi^+\pi^-$ or $\psi \to K^+K^-$. If the ψ were the eighth component of the octet, or a mixture, the $\psi \to \pi^+\pi^-$ decay is still forbidden, but the decays $\psi \to K^+K^-$ and $\psi \to K_SK_L$ occur with equal rates. For second order electromagnetic decays, exact SU_3 forbids the $\psi \to \gamma \to K_SK_L$ decay. Thus, the absence of the $\psi \to K_SK_L$ decay would support the singlet hypothesis. An upper limit of 0.02% for this decay mode has been set.

The decay mode $\psi \to \Lambda\bar{\Lambda}$ has also been seen, with a branching ratio of 0.16 ± 0.08%. The approximate equality of the $\psi \to \Lambda\bar{\Lambda}$ branching ratio with the $\psi \to p\bar{p}$ branching ratio also supports the singlet hypothesis. However, the ratio of KK^* to $\pi\rho$ decays is in disagreement with the singlet predictions.

ψ' HADRONIC DECAYS

The ψ' decays predominantly to the ψ with the emission of two pions.[12] While this decay mode has been studied, almost nothing is known about other decay modes, except that they do not seem to be simple.

The mode $\psi' \to \psi$ + anything is studied by observing the leptonic decay of the ψ. The mode $\psi' \to \psi + X$, $\psi \to \mu^+\mu^-$ is shown distinctly in Figure 4b, which shows the invariant mass distribution of μ pairs from ψ decays. The high mass peak is from the QED and resonant production of muon pairs, and the well separated

TABLE II

Decay Modes of the $\psi(3095)$

Mode	Branching Ratio (%)	No. of Events Observed	Comments
e^+e^-	6.9 ± 0.9	ca 2000	
$\mu^+\mu^-$	6.9 ± 0.9	ca 2000	
$\rho\pi$	1.3 ± 0.3	153 ± 13	$>70\%$ of $\pi^+\pi^-\pi^o$
$2\pi^+ 2\pi^-$	0.4 ± 0.1	76 ± 9	
$2\pi^+ 2\pi^- \pi^o$	4.0 ± 1.0	675 ± 40	20% $\omega\pi^+\pi^-$ 30% $\rho\pi\pi\pi$
$3\pi^+ 3\pi^-$	0.4 ± 0.2	32 ± 7	
$3\pi^+ 3\pi^- \pi^o$	2.9 ± 0.7	181 ± 26	
$4\pi^+ 4\pi^- \pi^o$	0.9 ± 0.3	13 ± 4	
$\pi^+\pi^- K^+K^-$	0.4 ± 0.2	83 ± 18	not including $K^*(892)$ K^* (1420)
$2\pi^+ 2\pi^- K^+K^-$	0.3 ± 0.1		
$K_S K_L$	<0.02	≤ 1	90% C.L.
$K^o K^{o*}(892)$	0.24 ± 0.05	57 ± 12	
$K^\pm K^{\mp*}(892)$	0.31 ± 0.07	87 ± 19	
$K^o K^{o*}(1420)$	<0.19	≤ 3	90% C.L.
$K^\pm K^{\mp*}(1420)$	<0.19	≤ 3	90% C.L.
$K^{*o}(892)\bar{K}^{*o}(892)$	<0.06	≤ 3	90% C.L.
$K^{*o}(1420)\bar{K}^{*o}(1420)$	<0.18	≤ 3	90% C.L.
$K^{*o}(892)K^{*o}(1420)$	0.37 ± 0.10	30 ± 7	
$p\bar{p}$	0.21 ± 0.04	105 ± 11	assuming $f(\theta) \sim 1+\cos^2\theta$
$\Lambda\bar{\Lambda}$	0.16 ± 0.08	19 ± 5	
$p\bar{p}\pi^o$ $\bar{n}p\pi^-$ $\bar{p}n\pi^+$	0.37 ± 0.19	87 ± 30	

lower peak is due to the ψ decay. Using the previously measured branching ratio for $\psi \to \mu^+\mu^-$, we find:

$$\frac{\Gamma(\psi' \to \psi + \text{anything})}{\Gamma(\psi \to \text{all})} = 0.57 \pm 0.08$$

The ψ may also be identified by calculating the mass recoiling against a pion pair, as in the decay $\psi' \to \psi + \pi^+ + \pi^-$. The mass recoiling against all pairs of charged particles is shown in Fig. 15a, revealing a sharp spike at a mass of 3.1 GeV, with a width equal to that expected from the detector momentum resolution. Folding the calculated detection efficiencies with this yield leads to:

$$\frac{\Gamma(\psi' \to \psi + \pi^+ + \pi^-)}{\Gamma(\psi \to \text{all})} = 0.32 \pm 0.04$$

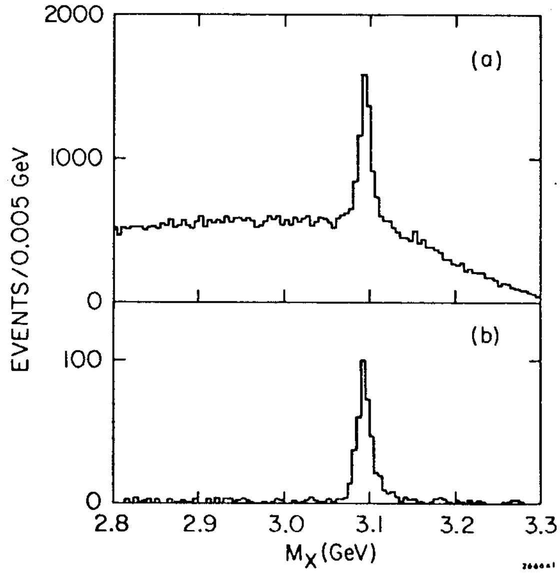

Fig. 15 a) Invariant mass M_X recoiling against all pairs of oppositely charged particles.
b) Same as (a) but for those events in which the observed charged particles satisfy, within errors, conservation of total momentum and energy.

These two branching ratios may be combined to find the fraction of $\psi' \to \psi$ cascades with a charged pion pair:

$$\frac{\Gamma(\psi' \to \psi + \pi^+ + \pi^-)}{\Gamma(\psi' \to \psi + \text{anything})} = 0.56 \pm 0.03$$

If the "anything" consists of only the charged pions and π^0 pairs, then the isospin of the pion system determines the above ratio. Values of approximately[13] 2/3, 1, and 1/3 correspond to isospin states of 0, 1, and 2, respectively. The isospin assignment 0 is preferred. The apparent absence of a single π^0 cascade decay and the large fraction of cascade decays with two pions indicate that the ψ' and ψ have the same G-parity. If the $I = 0$ assignment is correct, then the difference between the branching ratio of 0.56 and the predicted values may indicate that

$$\frac{\Gamma(\psi' \to \psi + \text{not } \pi\pi)}{\Gamma(\psi \to \psi + \text{anything})} \leq 10\% \ .$$

Figure 15b shows events where all the final particles in the decay $\psi' \to \psi + \pi^+\pi^-$ ($\psi \to \mu^+\mu^-$) are observed. There is almost no background, and these data have been used to study the angular distributions. The data appear to indicate that the dipion is in an S-wave state with respect to the leptons.

A small signal seems to be seen for the decay $\psi' \to \psi + \eta$ with a branching ratio of 4 ± 2%. Upper limits on the radiative decay of the ψ' to an intermediate state are approximately 7%. Such states might be the $3P_{0,1,2}$ states expected in the charmonium models of the ψ's.[14]

Approximately forty percent of the ψ' decays remain unaccounted for. It is interesting to remove the cascade decays from the ψ' sample and compare it with the ψ. This has been done for the class of 4-prong, Q = 0 events in Fig. 16. Each scatter plot displays the missing momentum against the total charged energy observed in each event, assuming pion kinematics. Figure 16a shows the ψ decays. The concentrations against the energy axis are the four body decays: $\pi^+\pi^-\pi^+\pi^-$ at E = 3.1 GeV, $\pi^+\pi^-K^+K^-$ around 2.8 GeV, and various combinations of π's, K's, and nucleons at lower energies. The strong diagonal concentration corresponds to $\pi^+\pi^-\pi^+\pi^-\pi^0$ decays. (b) shows the full sample of ψ' decays, and (c) shows the pion cascade decay. (d) shows (b) with the cascade contribution removed. Very little structure is left, but these decays are still being actively investigated. Upper limits on the decays $\rho^0\pi^0$ and $\pi^+\pi^-\pi^+\pi^-\pi^0$ have been set. It appears that the decays into odd numbers of pions are suppressed in comparison with the ψ. Perhaps there is some new principle or dynamics that ensures two neutrals in all the final states. A summary of the ψ' decay modes is listed in Table III.

OTHER STRUCTURES

Measurements of the total cross section σ_h now extend to an $E_{c.m.}$ of 7.4 GeV, and are shown in Figure 17. The principal structure is the peak at about 4.1 GeV.[15] The width is about 250-300 MeV, and it has a peak cross section of about 32 nb sitting on a background level of about 18 nb. If this structure is a resonance, its width and peak cross section are very different from the ψ's. However, the integrated cross section is about 5500 nb-MeV, a value

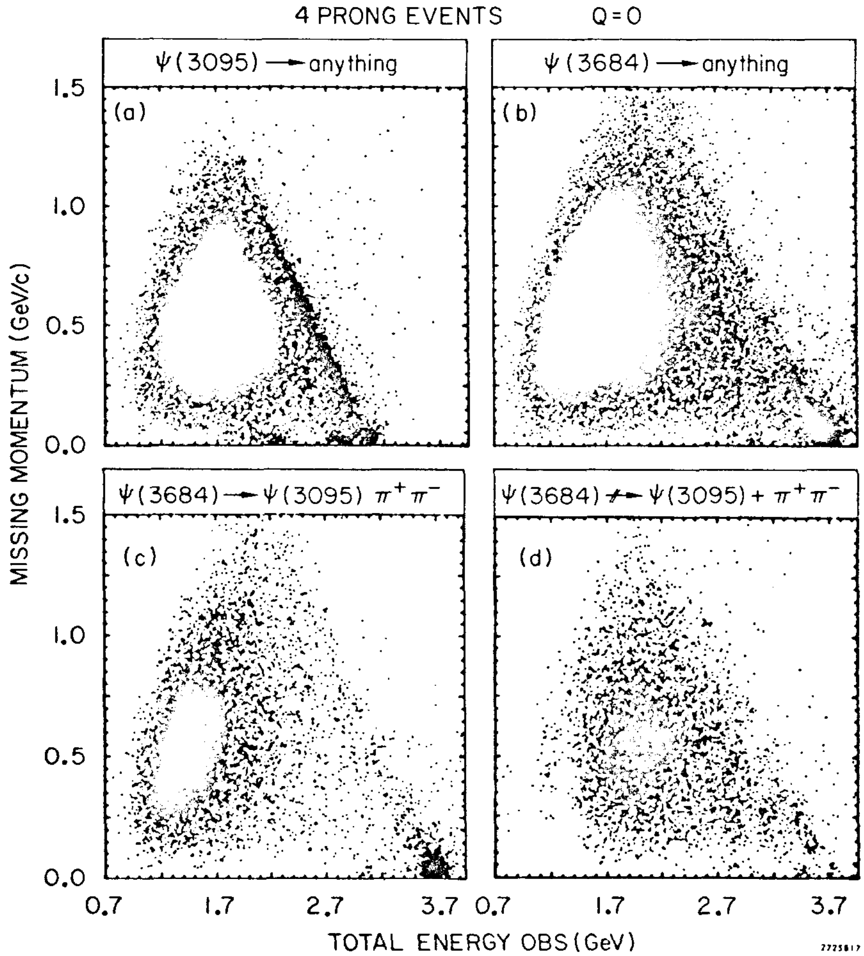

Fig. 16 Comparison of 4-prong events at the ψ and ψ'. Missing momentum versus total charged energy, assuming pion kinematics.

a) All 4-prongs at the ψ.
b) All 4-prongs at the ψ'.
c) All 4-prong $\psi' \rightarrow \psi + \pi^+\pi^-$ cascade decays.
d) Non-cascade ψ' decays, i.e., (c) removed from (b).

comparable with the ψ's. The study of exclusive decay modes from the 4.1 GeV structure is just beginning. The problem is complicated by the much smaller data sample here compared with the ψ's, because the peak cross section at 4.1 GeV is a relatively civilized 32 nb.

Other sharp structure has been sought.[16] Shortly after the discovery of the ψ, SPEAR and the magnetic detector were modified to allow scanning

TABLE III

Decay Modes of the $\psi(3684)$

Mode	Branching Ratio (%)	Comments
e^+e^-	0.97 ± 0.16	μ-e universality assumed
$\mu^+\mu^-$	0.97 ± 0.16	
$\psi(3095)$ anything	57 ± 8	
$\psi(3095)\ \pi^+\pi^-$	32 ± 4	these decays are included in the fraction for ψ + anything via an intermediate state
$\psi(3095)\ \eta$	4 ± 2	
$\psi(3095)\ \gamma\gamma$	< 6.6*	
$\rho^o\pi^o$	< 0.1*	
$2\pi^+ 2\pi^- \pi^o$	< 0.7*	* 90% confidence limit based on a preliminary analysis
$p\bar{p}$	< 0.03*	

measurements of the cross section in steps of c.m. energy of approximately 1.9 MeV. The time spent at each step was sufficient for the production of 1-2 hadronic events; this was typically a minute. The data were subject to the "off-line" analysis in real time and cross sections were determined after each step.

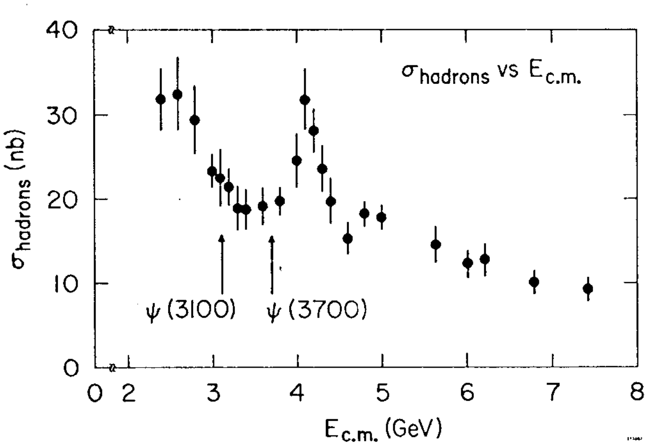

Fig. 17 Total hadron cross section vs. $E_{c.m.}$.

The ψ' was discovered by this system in its first few hours of use. Since then, the region between 3.2 GeV and 5.9 GeV has been scanned, as shown in Fig. 18. The scan has since been extended to 7.6 GeV. The sensitivity of the scan was such that a narrow resonance with an integrated strength between 5 and 10% of that of the ψ would have been seen. A set

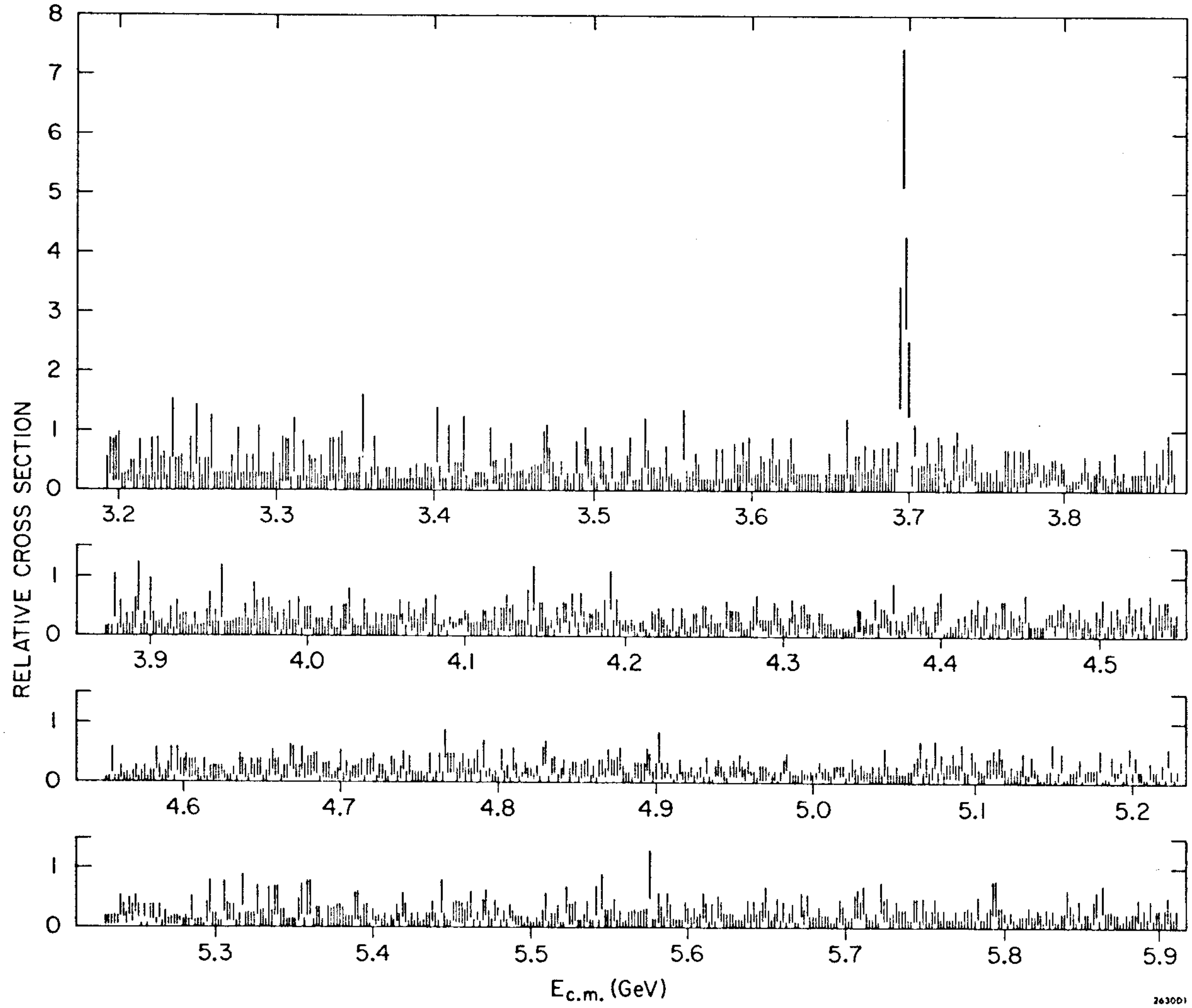

Fig. 18 Relative cross sections for e^+e^- into hadrons from the fine mesh narrow resonance search.

of upper limits for narrow resonances is shown in Table IV.

SUMMARY AND QUESTIONS

The ψ and ψ' seem to couple directly to photons, and have quantum numbers $J^{PC} = 1^{--}$. Both have odd G-parity and isospin zero. Photoproduction of the ψ at SLAC[17)] and FNAL[18)] implies a ψ-nucleon cross section of about 1 mb. These results seem consistent with the idea that the ψ's are hadrons.

On the other hand, one must contend with the narrow widths of the ψ's, about 70 keV for the ψ and 225 keV for the ψ'. At this time, no thoroughly satisfying theoretical explanation has emerged for the existence and properties of

TABLE IV

Results of the search for narrow resonances. Upper limits (90% confidence level) for the radiatively corrected integrated cross section of a possible narrow resonance. The width of this resonance is assumed to be small compared to the mass resolution.

Mass Range (GeV)	Limit on $\int \sigma_H \, dE_{cm}$ (nb MeV)
3.20 → 3.50	970
3.50 → 3.69	780
3.72 → 4.00	850
4.00 → 4.40	620
4.40 → 4.90	580
4.90 → 5.40	780
5.40 → 5.90	800
5.90 → 7.60	450

the ψ's. The leading contenders appear to be color and charm.[19] The color theories forbid strong decays of the ψ's because of a new nonadditive quantum number, so that electromagnetic decays with the emission of a photon would be expected. No evidence for such decays is seen. For example, in the four pion plus neutral decay of the ψ, there is a strong $\omega\pi\pi$ signal, indicating that the neutral is a π^0 and not a γ. The charm theories are based on the existence of a new additive quantum number, and rely on Zweig's[19] rule to suppress strong decays. The charm schemes imply the existence of many other states. A search[20] for some of these charmed states was performed at SPEAR and no evidence for them was found.

Another open question is to the meaning of the structure at 4.1 GeV. Is it another resonance related to the ψ and ψ' but having decay modes kinematically inaccessible to the ψ's? Are the resonances related to the step in $R = \sigma_h/\sigma_\mu$ around 4 GeV? Many questions have been raised by these data in the past few months - perhaps the next few months will see answers.

REFERENCES AND FOOTNOTES

1) J.-E. Augustin et al., Phys. Rev. Letters 33, 1406 (1974).
J. J. Aubert et al., Phys. Rev. Letters 33, 1404 (1974).
C. Bacci et al., Phys. Rev. Letters 33, 1408 (1974).

2) G. S. Abrams et al., Phys. Rev. Letters 33, 1453 (1974).

3) SPEAR Storage Ring Group, Proc. IXth Int. Conf. on High Energy Accelerators, Stanford Linear Accelerator Center, 1974, pp. 37-42.

4) The members of the SLAC-LBL Collaboration are: A. M. Boyarski, M. Breidenbach, F. Bulos, G. J. Feldman, G. E. Fischer, D. Fryberger, G. Hanson, D. L. Hartill, B. Jean-Marie, R. R. Larsen, D. Lüke, V. Lüth, H. L. Lynch, D. Lyon, C. C. Morehouse, J. M. Paterson, M. L. Perl, T. P. Pun, P. Rapidis, B. Richter, R. F. Schwitters, W. Tanenbaum, and F. Vannucci (Stanford Linear Accelerator Center); G. S. Abrams, D. D. Briggs, W. Chinowsky, C. E. Friedberg, G. Goldhaber, J. A. Kadyk, A. M. Litke, B. A. Lulu, F. M. Pierre, B. Sadoulet, G. H. Trilling, J. S. Whitaker, F. Winkelmann, and J. E. Wiss (Lawrence Berkeley Laboratory).

5) A. M. Boyarski et al., Phys. Rev. Letters 34, 1357 (1975).

6) It is possible that the muon sample has a small hadronic contamination. Muon identification relies on shower counter information, aided by penetration of the muon through 20 cm of iron. Collinear pion pairs could be mistaken for muon pairs.

7) A. M. Boyarski et al., to be published.

8) These values for the QED cross sections reflect the cut $|\cos\theta| < 0.6$.

9) D. R. Yennie, Phys. Rev. Letters 34, 239 (1975).

10) There is no strong evidence for the decay mode $\psi \to \pi^+\pi^-\pi^+\pi^-\gamma$. Aside from the missing mass peak being located slightly above a mass of zero, these events show a strong $\omega\pi\pi$ and $\rho\pi\pi\pi$ clustering.

11) F. J. Gilman, private communication.

12) G. S. Abrams et al., Phys. Rev. Letters 34, 1177 (1975).

13) There are small phase space corrections to the ratios predicted from the isospins.

14) C. Callen et al., Phys. Rev. Letters 34, 52 (1975).
T. Appelquist et al., Phys. Rev. Letters 34, 365 (1975).
E. Eichten et al., Phys. Rev. Letters 34, 369 (1975).

15) J.-E. Augustin et al., Phys. Rev. Letters 34, 764 (1975).

16) A. M. Boyarski et al., Phys. Rev. Letters 34, 762 (1975).

17) J. T. Dakin et al., Phys. Letters 56B, 405 (1975).
U. Camerini et al., SLAC-PUB-1591 (1975), submitted to Phys. Rev. Letters.

18) B. Knapp et al., Phys. Rev. Letters 34, 1040 (1975); ibid., p. 1044.

19) For a review of these theories, see H. Harari, SLAC-PUB-1514, unpublished; F. J. Gilman, SLAC-PUB-1537 (1975), to be published in Proc. Orbis Scientiae II, Coral Gables, Florida, 1975; O. W. Greenberg, University of Maryland Technical Report No. 75-064, to be published in Proc. Orbis Scientiae II, Coral Gables, Fla., 1975.

20) A. M. Boyarski et al., SLAC-PUB-1583 (1975), submitted to Phys. Rev. Letters.

APPENDIX I

The storage ring SPEAR circulates one bunch of electrons and one bunch of positrons in a single magnetic guide field. The bunches collide alternately in two interaction regions. The beam energies may now be varied between about 1.3 GeV and 4 GeV. The energy distribution of electrons within a beam bunch is approximately Gaussian with a width that increases approximately quadratically with energy, and has a σ of about 1 MeV at a total energy ($E_{c.m.} = 2E_{beam}$) of $E_{c.m.} = 3$ GeV. The absolute energy calibration is based on measurements of the particle orbits and the magnetic guide fields and is known to about 0.1%. The bunch shapes are Gaussian with σ's in the transverse plane of approximately 0.1 cm and longitudinally a few cm. The luminosity is about $3 \times 10^{29} cm^{-2} sec^{-1}$ at $E_{c.m.} = 3$ GeV.

The magnetic detector is shown schematically in Fig. 1. The magnetic field of 4 kilogauss is axial and within a volume about 3 meters in diameter by 3 meters long. The interaction region is surrounded by a stainless steel vacuum pipe 0.15 mm thick. Coaxial with the pipe are a pair of cylindrical plastic scintillation counters that form one element of the trigger system. Continuing radially outward are four sets of multiwire spark chambers. Each set consists of four layers of wires at $\pm 2^o$ and $\pm 4^o$ with respect to the beam axis. Thus, each set of chambers provides redundant azimuthal (resolution ≈ 0.5 mm) and longitudinal (resolution ≈ 1.2 cm) position information for each charged particle. Following the spark chambers are a set of 48 plastic scintillator trigger counters. These counters are used in the trigger system and in a time-of-flight particle identification system with a resolution (σ) of about 0.5 nsec, allowing π/K separation up to about 0.65 GeV/c. Next comes the aluminum coil of the solenoid with a thickness of about 1 radiation length, followed by a layer of 24 lead-scintillator sandwich electron shower counters used to identify electrons. The next element is the iron return yoke of the magnet, which also serves as a hadron filter for the final set of spark chambers which aid in muon identification.

The accuracy of single particle identification in the detector is momentum dependent. Above about 600 MeV/c the probability of mistaking an electron for a hadron is about 6%, an electron for a muon about 1%, and a muon for a hadron about 8%. In the momentum range 600 MeV/c to 900 MeV/c, the probabilities of hadrons mimicking electrons or muons are 13% and 16%, respectively.

The trigger requirement is two or more charged particles with transverse momenta greater than about 200 MeV/c. The complete detector system covers a solid angle of $0.65 \times 4\pi$. A hadronic event is defined to be one with 3 charged particles or two charged particles acollinear by 20° or more. The detection efficiency for hadronic events varies smoothly from 40% at $E_{c.m.}$ = 2.5 GeV to 65% at 7.0 GeV. Backgrounds have been studied using separated beams and longitudinal (z) distributions of events. The background contribution to the resonances is very small, of order 0.1%, and is roughly 5% in the nonresonant region. Normally, cross sections are normalized by measuring Bhabha scattering in the magnetic detector. However, in the vicinity of the ψ, the e^+e^- pair production cross section is strongly enhanced by "2nd order electromagnetic" decays of the resonance. Hence, the luminosity is integrated by a set of small counters monitoring Bhabha scattering at small angles (where the scattering is dominantly caused by space-like photons). The luminosity monitor is calibrated with the magnetic detector at a beam energy far from the resonances.